molecules

MDPI

Article

Synthesis of Chromium(II) Complexes with Chelating Bis(alkoxide) Ligand and Their Reactions with Organoazides and Diazoalkanes

Sudheer S. Kurup [1], Richard J. Staples [2], Richard L. Lord [3,*] and Stanislav Groysman [1,*]

1 Department of Chemistry, Wayne State University, 5101 Cass Ave., Detroit, MI 48202, USA; sudheer.kurup@wayne.edu
2 Department of Chemistry, Michigan State University, 578 S Shaw Ln, East Lansing, MI 48824, USA; staples@chemistry.msu.edu
3 Department of Chemistry, Grand Valley State University, 1 Campus Dr, Allendale, MI 49401, USA
* Correspondence: lordri@gvsu.edu (R.L.L.); groysman@wayne.edu (S.G.)

Academic Editor: Klaus Banert
Received: 12 December 2019; Accepted: 7 January 2020; Published: 9 January 2020

Abstract: Synthesis of new chromium(II) complexes with chelating bis(alkoxide) ligand $[OO]^{Ph}$ ($H_2[OO]^{Ph}$ = [1,1′:4′,1′′-terphenyl]-2,2′′-diylbis(diphenylmethanol)) and their subsequent reactivity in the context of catalytic production of carbodiimides from azides and isocyanides are described. Two different Cr(II) complexes are obtained, as a function of the crystallization solvent: mononuclear $Cr[OO]^{Ph}(THF)_2$ (in toluene/THF, THF = tetrahydrofuran) and dinuclear $Cr_2([OO]^{Ph})_2$ (in CH_2Cl_2/THF). The electronic structure and bonding in $Cr[OO]^{Ph}(THF)_2$ were probed by density functional theory calculations. Isolated $Cr_2([OO]^{Ph})_2$ undergoes facile reaction with 4-$MeC_6H_4N_3$, 4-$MeOC_6H_4N_3$, or 3,5-$Me_2C_6H_3N_3$ to yield diamagnetic Cr(VI) bis(imido) complexes; a structure of $Cr[OO]^{Ph}(N(4\text{-}MeC_6H_4))_2$ was confirmed by X-ray crystallography. The reaction of $Cr_2([OO]^{Ph})_2$ with bulkier azides N_3R ($MesN_3$, AdN_3) forms paramagnetic products, formulated as $Cr[OO]^{Ph}(NR)$. The attempted formation of a Cr–alkylidene complex (using N_2CPh_2) instead forms chromium(VI) bis(diphenylmethylenehydrazido) complex $Cr[OO]^{Ph}(NNCPh_2)_2$. Catalytic formation of carbodiimides was investigated for the azide/isocyanide mixtures containing various aryl azides and isocyanides. The formation of carbodiimides was found to depend on the nature of organoazide: whereas bulky mesitylazide led to the formation of carbodiimides with all isocyanides, no carbodiimide formation was observed for 3,5-dimethylphenylazide or 4-methylphenylazide. Treatment of $Cr_2([OO]^{Ph})_2$ or $H_2[OO]^{Ph}$ with NO^+ leads to the formation of [1,2-b]-dihydroindenofluorene, likely obtained via carbocation-mediated cyclization of the ligand.

Keywords: alkoxides; azides; carbodiimides

1. Introduction

Organoazides constitute efficient and sustainable precursors for the formation of reactive nitrene functionality, which engenders many useful transformations, including C–H bond amination, aziridination, formation of azoarenes and carbodiimides, and others [1–7]. Transition metals generally enable milder conditions for the formation of nitrenes and higher selectivity in their subsequent transfer. The majority of nitrene-transfer studies are focused on middle and late transition metals, which generally feature weaker metal–imido bonds and therefore exhibit more reactive nitrene functionalities [8–21]. In contrast, early transition metals (particularly chromium) typically exhibit less reactive nitrene functionalities due to the stability of multiple metal-nitrogen bonds [22–28]. However, recent studies demonstrated the ability of coordinatively unsaturated chromium(IV)–imido to transfer

nitrene to olefins or isocyanides to form aziridines and carbodiimides, respectively [29–31]. C–C and C–H bond activation reactions featuring reactive chromium(IV)–imido were also reported [32]. As part of our ongoing investigation of nitrene- and carbene-transfer chemistry mediated by 3d metal complexes in bulky alkoxide ligand environments [33,34], we have reported the synthesis and reactions of chromium–imido complexes featuring two bulky monodentate alkoxides [OC^{t}Bu$_2$Ph] [31]. We have demonstrated that Cr^{IV}(OC^{t}Bu$_2$Ph)$_2$(NR′) complexes, which were formed for bulky R′ groups (R′ = Mes, 2,6-Et$_2$C$_6$H$_3$, 1-adamantyl), enabled catalytic transfer of the nitrene group [NR′] to isocyanides to form carbodiimides. In contrast, the reaction of less bulky *para*-substituted aryl azides N$_3$R′ (R′ = 4-MeC$_6$H$_4$, 4-MeOC$_6$H$_4$, 4-CF$_3$C$_6$H$_4$) formed Cr(VI) complexes Cr^{VI}(OR)$_2$(NR′)$_2$ that were catalytically inactive. Recently, we have reported a new chelating bis(alkoxide) ligand [OO]^{Ph} [35] that created a similar bis(alkoxide) ligand environment but warranted a higher degree of stability of the resulting iron complex Fe[OO]^{Ph}, and consequently led to a broader range of catalytic nitrene transfer compared with related Fe(OR)$_2$ systems [36,37]. Herein, we report our synthetic, structural, and catalytic studies on the chemistry of Cr^{II}[OO]^{Ph} with organoazides and diazoalkanes and compare this reactivity with the previously reported Cr^{II}(OC^{t}Bu$_2$Ph)$_2$ system.

2. Results and Discussion

2.1. Synthesis and Structures of Cr(II) Precursors

Treatment of the chromium(II) amide precursor with one equivalent of H$_2$[OO]^{Ph} in THF produces a green solid. Recrystallization of the product from the toluene/THF mixture yields mononuclear pale green Cr[OO]^{Ph}(THF)$_2$ (**1**) related to the mononuclear Cr(OC^{t}Bu$_2$(3,5-Ph$_2$C$_6$H$_3$))$_2$(THF)$_2$ [38]. In contrast, recrystallization of the product from a mixture of two polar solvents (CH_2Cl_2 and THF) forms pale green–blue homodinuclear complex Cr$_2$[OO]$^{Ph}_2$ (**2**, Scheme 1) isolated in 79% yield. Homodinuclear complex **2** is structurally related to the previously reported alkoxide-bridged Cr$_2$(OC^{t}Bu$_2$Ph)$_4$ [31], Cr$_2$(OC^{t}Bu$_3$)$_2$(μ^2-OC^{t}Bu$_2$H)$_2$ [39], and siloxide-bridged Cr$_2$(OSi^{t}Bu$_3$)$_4$ [40]. We note that monodentate alkoxides [OC^{t}Bu$_2$Ph] and [OC^{t}Bu$_2$(3,5-Ph$_2$C$_6$H$_3$)] formed dinuclear or mononuclear complexes selectively [31,38], whereas the chelating ligand appears to support both types of geometries in the solid state, depending on the nature of the crystallization medium.

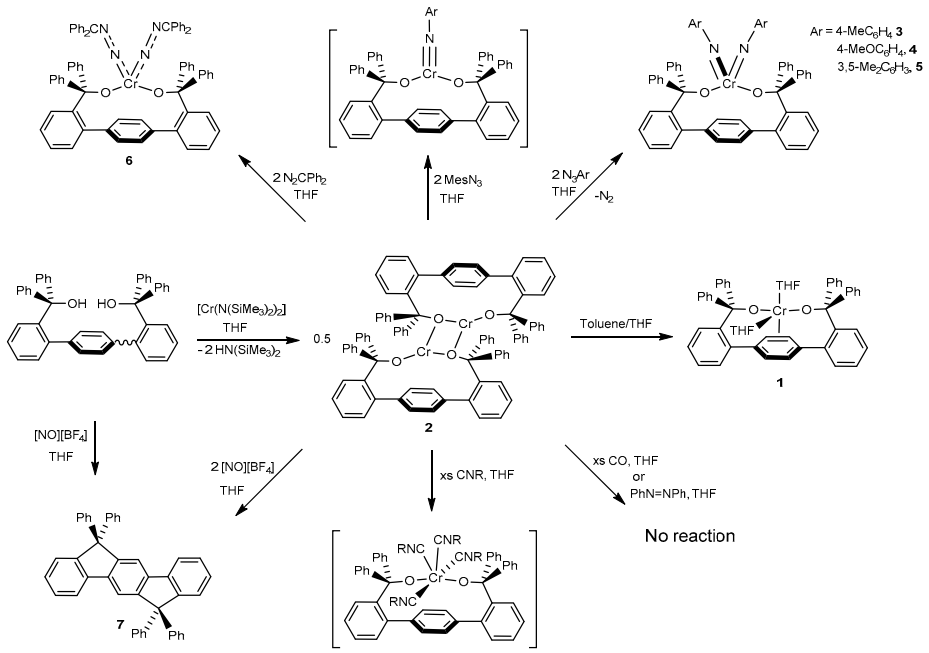

Scheme 1. Synthesis and reactivity of Cr(II) complexes in the chelating bis(alkoxide) ligand environment.

The structures of complexes **1** and **2** are given in Figure 1. The structure of **1** is similar to the previously reported structure of $Fe[OO]^{Ph}(THF)_2$ [35]. However, the structure of $Fe[OO]^{Ph}(THF)_2$ exhibited a very long distance between the metal and the central phenyl (>3 Å), indicating no interaction [35]. In contrast, the distance between the chromium center and the central phenyl in **1** is 2.49(1) Å, which suggests bonding between the metal and the phenyl ring. The inter-alkoxide RO-Cr-OR and THF-Cr-THF angles are 173.6(2)° and 88.1(2)°, respectively. Two independent molecules of homodinuclear complex **2** were found in the asymmetric unit exhibiting similar structural parameters; only one is shown. Each $[OO]^{Ph}$ ligand provides one terminal and one bridging alkoxide donor; no coordination to the central phenyl is observed in this case (Cr—Ph ≥ 3.0 Å). While the overall geometry and metrics in **2** are similar to those of $Cr_2(OC^tBu_2Ph)_4$ and related complexes [32,39,40], the metal centers in **2** exhibit significant distortion of trigonal planar geometry, as indicated by the considerable difference in O-Cr-O angles (Figure 2) and displacement of Cr from the trigonal plane (varies between 0.105 and 0.348 Å).

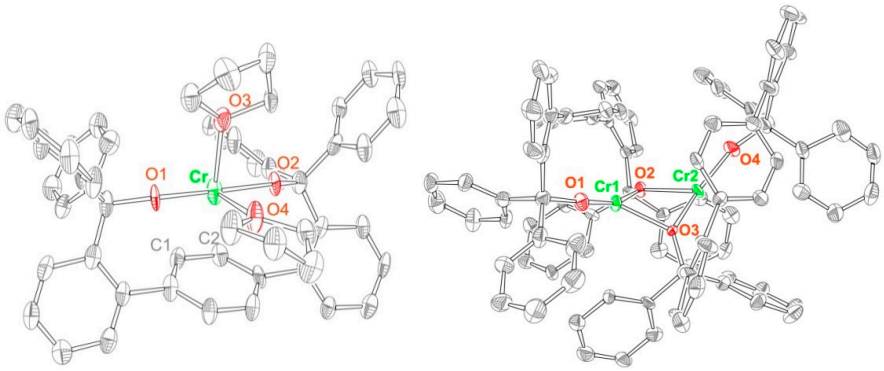

Figure 1. X-ray structures of **1** (left) and **2** (right), 50% probability ellipsoids. H atoms and co-crystallized solvent molecules were omitted for clarity. Selected bond distances (Å) and angles (°) for **1**: Cr O1, 1.924(6), Cr O2, 1.935(6), Cr O3, 2.156(7), Cr O4, 2.277(6), Cr — Ph 2.49(1), O1 Cr1 O2, 173.6(2), O1 Cr1 O3, 86.7(2), O2 Cr1 O3, 90.0(3), O1 Cr1 O4, 85.9(2), O2 Cr1 O4, 88.5(2), O3 Cr1 O4, 88.1(2). Selected bond distances (Å) and angles (°) for **2**: Cr1 O1, 1.788(5), Cr2 O4, 1.799(5), Cr1 O2, 1.976(5), Cr1 O3, 2.013(6), Cr2 O3, 1.981(5), Cr2 O2, 2.049(5), Cr1 — Cr2, 2.896(2), O2 Cr1 O3, 81.2(2), O1 Cr1 O2, 150.2(3), O1 Cr1 O3, 120.1(2).

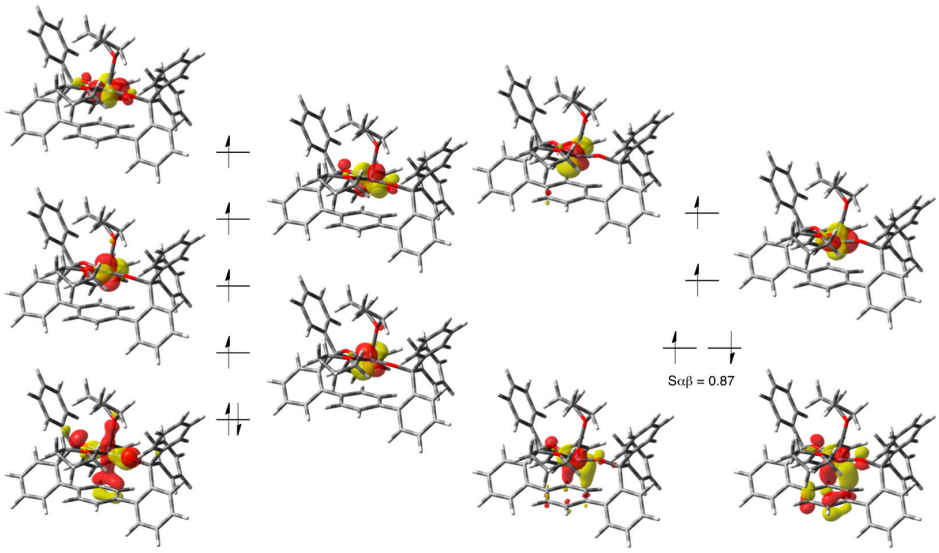

Figure 2. Corresponding orbital diagrams for $\mathbf{1_Q}$ (left) and $\mathbf{1_T}$ (right) at the BP86-D3/def2-SVP level of theory. Orbitals are plotted with an isosurface value of 0.05 au.

To better understand the electronic structure and bonding in **1**, density functional theory (DFT) calculations were performed. Singlet ($\mathbf{1_S}$), triplet ($\mathbf{1_T}$), and quintet ($\mathbf{1_Q}$) states were optimized. $\mathbf{1_Q}$ is lowest in free energy, followed by $\mathbf{1_T}$ at 19.7 kcal/mol, and $\mathbf{1_S}$ at 28.6 kcal/mol. The optimized structure of $\mathbf{1_Q}$ agrees well with the crystallographically determined structure and has bond lengths of Cr–O1 = 1.915 Å, Cr–O2 = 1.928 Å, Cr–O3 = 2.203 Å, Cr–O4 = 2.281 Å, Cr–C1 = 2.475 Å, and Cr–C2 = 2.525 Å; both $\mathbf{1_T}$ and $\mathbf{1_S}$ are inconsistent with the x-ray data (Table S1, SI). Based on the spin density localized at Cr, $\mathbf{1_Q}$ is best described as a high-spin Cr(II) species. Similar to what was observed in the optimization of different spin states of Fe[OO]^{Ph}(THF)$_2$ [35], the higher-energy, lower spin states $\mathbf{1_T}$/$\mathbf{1_S}$ exhibit much shorter Cr–phenyl contacts of 2.1–2.2 Å. Mayer bond orders for Cr–C1/C2 are calculated to be 0.25 and 0.23 in $\mathbf{1_Q}$. In comparison, quintet Fe[OO]^{Ph}(THF)$_2$ (with Fe–C distances of 2.8–2.9 Å) has smaller bond orders of 0.06 and 0.09, whereas $\mathbf{1_T}$ has larger bond orders of 0.64 and 0.65. For perspective, M–O$_{THF}$ bond orders are 0.2–0.3 and the M–O$_{alkoxide}$ bond orders are 0.6–0.9. Frontier orbital diagrams of $\mathbf{1_Q}$ and $\mathbf{1_T}$ (Figure 2) illustrate the Cr–phenyl bonding in both spin states. The much stronger bonding in $\mathbf{1_T}$ is due to the *d*-π backbonding that is possible with intermediate-spin Cr(II) ion. This back-bonding is not significant in $\mathbf{1_Q}$ due to half-occupation of that *d*-orbital in the high-spin Cr(II) ion. Collectively, these computational data suggest a weak covalent interaction between Cr and the bridging phenyl moiety in **1**.

We have also investigated the structures of **1** and **2** in solution. Both compounds give rise to paramagnetic NMR spectra, as anticipated. The UV–Vis spectra of **1** and **2** (collected in THF) are very similar, exhibiting a peak at approximately 710 nm, and a shoulder at approximately 510 nm (Figures S39 and S40, SI). The solution magnetic moment of **1** (3.0(3) μB, C_6D_6) was found to be significantly lower than the expected spin-only value of 4.9 μB. Recalculated for the structure of Cr$_2$([OO]^{Ph})$_2$, the observed magnetic moment is 2.6(2) μB (per Cr), which is close to the observed value of 2.5(3) μB reported for Cr$_2$(OC^{t}Bu$_2$Ph)$_2$ [31]. These data suggest that **1** undergoes dimerization in solution to form **2**.

2.2. Reactions of Chromium(II) Complexes with Organoazides, Azoarenes and Diazoalkanes

Following the synthesis of the chromium(II) precursor, its reactivity with organoazides was investigated. Complex **2** was utilized as a precursor in group-transfer reactions. Similar to Cr$_2$(OC^{t}Bu$_2$Ph)$_4$ [31], **2** was found to exhibit profoundly distinct reactivity with non-bulky (*4*-tolyl, *4*-methoxyphenyl, and 3,5-dimethylphenyl) vs. bulky (mesityl, 1-adamantyl) organoazides. Treating a green solution of **2** with two equivalents of *para*-tolylazide in THF leads to a dark-brown solution, from which diamagnetic **3** is isolated in 69% yield by recrystallization from THF/ether. Similarly, treating **2** with two equivalents of 4-MeOC$_6$H$_4$N$_3$ or 3,5-Me$_2$C$_6$H$_3$N$_3$ forms brown solutions containing diamagnetic products **4** and **5** in 54% and 59%, respectively. We were not able to obtain X-ray quality crystals of **4** and **5**, however, their NMR and UV–Vis data (see SI) suggests similarity to **3**. The overall connectivity of **3** was confirmed by X-ray structure determination (Figure 3). The structure reveals a distorted tetrahedral geometry, consistent with Cr(VI) bis(imido) formulation. No chromium-phenyl interaction is observed in this case, with the chromium-phenyl distance exceeding 3.5 Å. As the structure was of relatively low quality, its metric parameters will not be further discussed.

In contrast, the reaction of the chromium(II) precursor with two equivalents of bulkier mesityl azide (per Cr) produces a paramagnetic brown solution, containing approximately one equivalent of unreacted azide. Similarly, treating chromium(II) precursor with two equivalents of 1-adamantyl azide also produces paramagnetic product, along with unreacted azide. We were not able to obtain X-ray quality crystals of the products. The formation of trigonal Cr(IV) mono(imido) complexes is proposed, based on similar formation of brown paramagnetic Cr^{IV}(OC^{t}Bu$_2$Ph)$_2$(NMes) and Cr^{IV}(OC^{t}Bu$_2$Ph)$_2$(NAd) upon reaction of [Cr(OC^{t}Bu$_2$Ph)$_2$] with excess azide. We note that selective formation of Cr(IV) mono(imido) complexes upon reaction with bulkier organoazides was also observed for the chromium(II) system ligated by two monodentate siloxides, [Cr(OSi^{t}Bu$_3$)$_2$] [40].

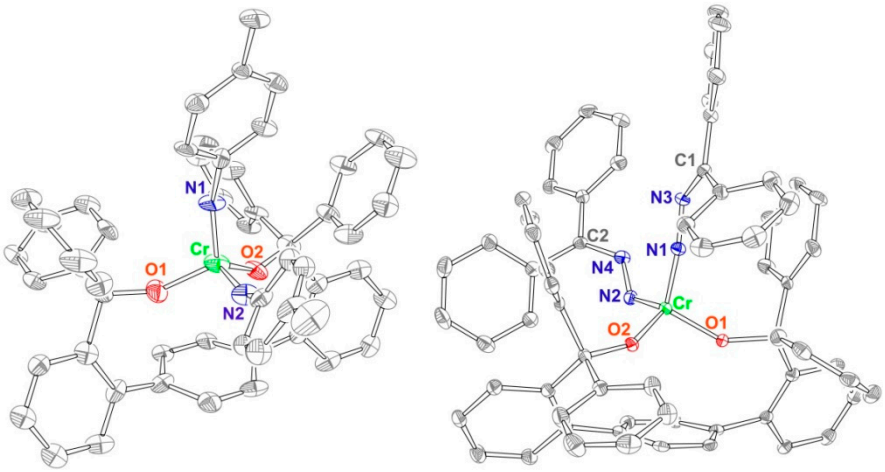

Figure 3. X-ray structure of **3** (left) and **6** (right), 50% probability ellipsoids. H atoms and co-crystallized solvent molecules were omitted for clarity. Selected bond distances (Å) for **6**: Cr O1 1.807(2), Cr O2 1.777(2), Cr N1 1.645(3), Cr N2 1.716(3), N1 N3 1.305(4), N2 N4 1.301(4). Selected bond angles (°): O2 Cr O1 110.0(1), N1 Cr N3 99.7(2), N1 Cr O2 110.5(1), N2 Cr O2 109.2(1), N1 Cr O1 113.1(1), Cr N1 N3 159.8(2), Cr N2 N4 131.2(2).

In addition to the reactions of Cr(II) precursor with organoazides, we have also studied its reactivity with azobenzene, with the goal to produce Cr(VI) bis(imido) via azobenzene cleavage. Cleavage of the N=N double bond in azoarenes at a single metal center is rare [41–44]. Heating the mixture of complex **2** with azobenzene to 60 °C in C_6D_6 for 24 h did not lead to the formation of $Cr^{VI}[OO]^{Ph}(NPh)_2$ as indicated by ^1H NMR spectroscopy.

Next, the reactivity of the Cr(II) bis(alkoxide) precursor with diazoalkanes was investigated, targeting formation of Cr(IV)/Cr(VI)-alkylidene complexes. Cr–alkylidene complexes are rare [26,45,46], and their reactivity is relatively unexplored. The related cobalt(II) bis(alkoxide) complex $Co(OC^tBu_2Ph)_2(THF)_2$ formed high-valent cobalt-alkylidene upon reaction with N_2CPh_2 and $N_2C(Ph)(CO_2Me)$ [47], whereas the corresponding iron complex $Fe(OC^tBu_2Ph)_2(THF)_2$ reductively coupled diazoalkanes/diazoesters via terminal nitrogens to form bridging tetrazene species [48]. A different reactivity mode was observed for the chromium bis(alkoxide). Treatment of **2** with diphenyldiazomethane results in the formation of brown $Cr[OO]^{Ph}(NNCPh_2)_2$ species (**6**), which was characterized by X-ray crystallography. The complex appears unstable in both solid state and solution. Our repeated attempts to collect the NMR spectrum of the X-ray quality crystals produced spectra with varying but significant decomposition products (benzophenone azine, free ligand); peaks attributable to the complex were broad and not informative. Wolczanski and coworkers have reported similar reactivity of $Cr_2(OSi^tBu_3)_4$ with N_2CPh_2 to yield $Cr(OSi^tBu_3)_2(N_2CPh_2)_2$ complex [40] and their complex also demonstrated limited stability.

The structure of **6** and selected metrics are given in Figure 3. The chromium center exhibits distorted tetrahedral geometry. Interestingly, the Cr–N bonds are different, one being significantly shorter (1.645(3) Å) than the other (1.716(3) Å). The shorter bond could be indicative of a higher metal-nitrogen bond order (triple), while the longer one suggests a metal-nitrogen double bond. The Cr–N–N bond angles of the [$NNCPh_2$] functionality are consistent with these formulations: for the triply bonded [Cr≡N1-N3] hydrazido, the angle is closer to linear (159.8(2) °), whereas for the doubly bonded [Cr=N2-N4] the angle is smaller (131.2(2) °). The N1-N3 and N2-N4 bonds are similar (1.304(4) vs. 1.301(4) Å), being intermediate between single and double. Similar dependence of the Cr–N–N angle within diphenylmethylenehydrazido functionalities on the chromium-nitrogen bond order was reported by Wolczanski, Cundari, and coworkers for the related $Cr(OSi^tBu_3)_2(=N_2CPh_2)_2$ [40]. The major difference between the present structure and the structure reported by Wolczanski is that in

$Cr(OSi^tBu_3)_2(=N_2CPh_2)_2$ the Cr–N bonds were similar (1.664(2) and 1.666(2) Å), leading to similar Cr–N–N bond angles (150.2(2) and 150.4(3) °).

DFT calculations on **6** were performed to analyze the electronic structure of this species. Singlet ($\mathbf{6_S}$), triplet ($\mathbf{6_T}$), and quintet ($\mathbf{6_Q}$) states were optimized and the singlet was found to be lowest in free energy followed by the triplet (+15.1 kcal/mol) then the quintet (+33.9 kcal/mol). Only the optimized structure of $\mathbf{6_S}$ is consistent with the experimental X-ray structure (Table S3, SI) and has no unpaired electrons. As the localized frontier orbitals in Figure 4 demonstrate, there are two -π-bonding interactions with the more linear diazoalkane ligand (HOMO–1/LUMO+3, HOMO–3/LUMO) compared to one with the less linear diazoalkane ligand (HOMO/LUMO+4), though the HOMO–1/LUMO+3 pair shows interaction with both diazoalkane ligands. The modest difference in Mayer bond orders of 1.61 vs. 1.52 for Cr–N1 vs. Cr–N2 suggests that both Cr–N bonds are between doubly and triply bonded, but that bonding to N1 is stronger.

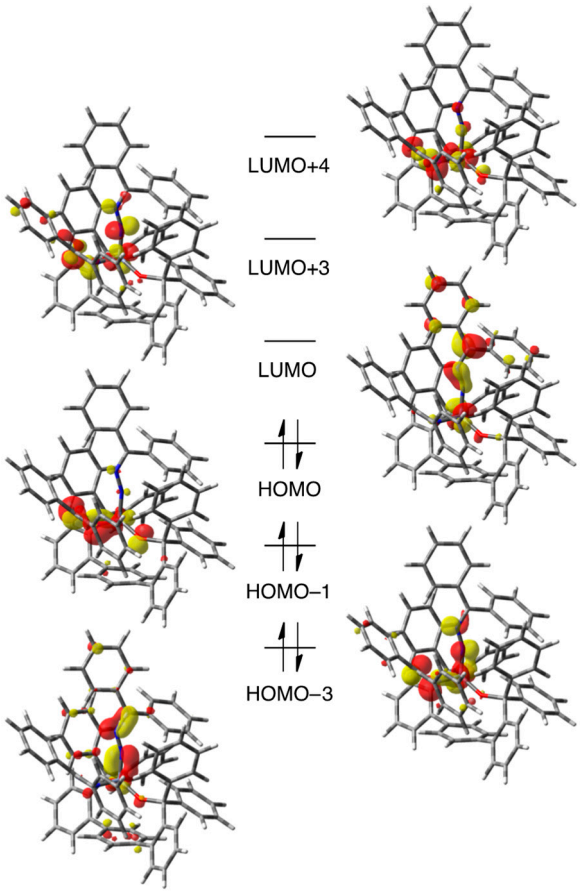

Figure 4. Frontier orbital diagram for $\mathbf{6_S}$ at the BP86-D3/def2-SVP level of theory. Orbitals are plotted with an isosurface value of 0.05 au.

2.3. Reactivity of Cr(II) with CO, CNR and NO^+

Following the investigation of the reactivity of Cr(II) bis(alkoxide) precursor with organoazides and diazoalkanes, its reactivity with isocyanides, carbon monoxide, and nitrosonium was explored next. It was previously shown that $Cr_2(OC^tBu_2Ph)_4$ reacted with isocyanides to form $Cr^{II}(OC^tBu_2Ph)_2(CNR)_4$ (R = 2,6-$Me_2C_6H_3$); formation of $Cr^{II}(OC^tBu_2Ph)_2(CNR)_4$ enabled subsequent development of the catalytic cycle for the production of carbodiimides. Hoping that the more stable and sterically demanding chelating bis(alkoxide) system will enable better catalytic reactivity in CNR and perhaps CO transfer, reactions of $Cr[OO]^{Ph}$ with xylyl isocyanide and carbon monoxide were investigated.

The reactivity of this species with nitrosonium ((NO)(BF_4)) was also studied, in light of the isoelectronic nature between NO^+ and CO/CNR.

Addition of excess xylyl isocyanide to the light-green solution of **2** (dissolved in THF) forms a brown solution immediately. ^{1}H NMR spectrum of the product indicates its paramagnetic nature. Although our multiple attempts to obtain X-ray quality crystals of the isocyanide product did not lead to fruition, the UV–Vis spectrum of the crude product is similar to the UV–Vis spectrum of isolated $Cr^{II}(OC^tBu_2Ph)_2(CN(2,6\text{-}Me_2C_6H_3))_4$ (peaks at approximately 400 and 460 nm, Figure S44) suggesting similarity of the products. In contrast, no color change was observed after treating the solution of **2** in THF with CO. Subsequent recrystallization from a toluene/THF mixture formed instead the crystals of compound **1**, further confirming the lack of reactivity with CO.

The reaction of **2** with NO^+ took an unexpected turn. Addition of (NO)(BF_4) to the green solution of **2** (THF) led to the development of cloudy yellow solution over the course of several hours. Subsequent recrystallization from THF yields colorless crystals of 6,6,12,12-tetraphenyl-6,12-dihydroindeno[1,2-b]fluorene **7** (Figure 5) isolated in 92% yield. The reaction course does not depend on the presence of Cr: treatment of the ligands precursor $H_2[OO]^{Ph}$ with (NO)(BF_4) yields the same product **7**. Cyclization of terphenyl bis(carbinol)s via carbocation intermediates to give various substituted dihydroindenofluorenes had been previously reported [49,50]. We surmise that the reaction proceeds via nitrosonium abstraction of hydroxyl (to yield nitrous acid) followed by cyclization, as described in Scheme 2.

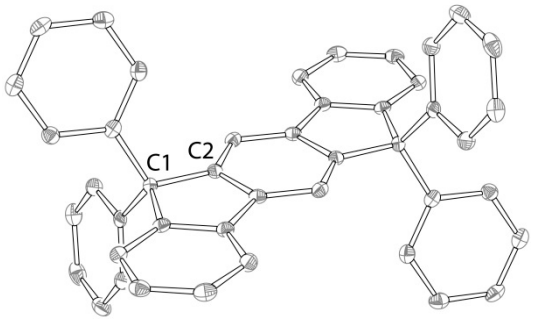

Figure 5. X-ray structure of **7**, 50% probability ellipsoids. H atoms and co-crystallized solvent molecules were omitted for clarity.

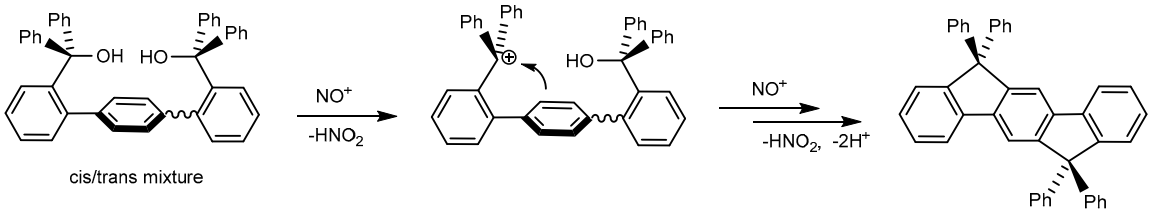

Scheme 2. Proposed cyclization mechanism of $H_2[OO]^{Ph}$.

2.4. Catalytic Reactivity in the Formation of Carbodiimides

Given the ability of the $Cr^{II}[OO]^{Ph}$ precursor to undergo stoichiometric reactions with organoazides and isocyanides, we investigated its catalytic reactivity in formation of carbodiimides. A matrix of four representative aryl azides of varying steric bulk (mesityl, 2-methylphenyl, 3,5-dimethylphenyl, and 4-methylphenyl) and four representative isocyanides (xylyl, 4-methoxyphenyl, 1-adamantyl, and cyclohexyl) was investigated (Scheme 3). All reactions were carried out in C_6D_6 at 60 °C for 24 h; the nature of the reaction products and their yields were determined by ^{1}H NMR spectroscopy. The outcome of the catalytic reaction appears to be a primary function of the organoazide. Catalytic formation of carbodiimides is observed for the bulkier mesityl azide. The reaction of mesityl azide with xylyl isocyanide gives nearly quantitative yield; good to moderate yields (72–50%) are observed for other

isocyanides. For the *ortho*-monosubstituted 2-methylphenyl azide, the reaction with xylyl isocyanide produces carbodiimide in a good yield, whereas other isocyanides give low yields of the corresponding products. No carbodiimide formation is observed for 3,5-dimethylphenyl azide and 4-methylphenyl azide. These results are rationalized by the nature of the chromium–imido intermediate, as was described in our previous study [31]. Whereas bulkier azide forms a chromium(IV)–imido, which is capable of isocyanide coordination and subsequent N-C bond formation, tetrahedral chromium(VI) bis(imido) (formed with non-bulky aryl azides) does not coordinate an isocyanide and therefore does not catalyze N-C bond formation.

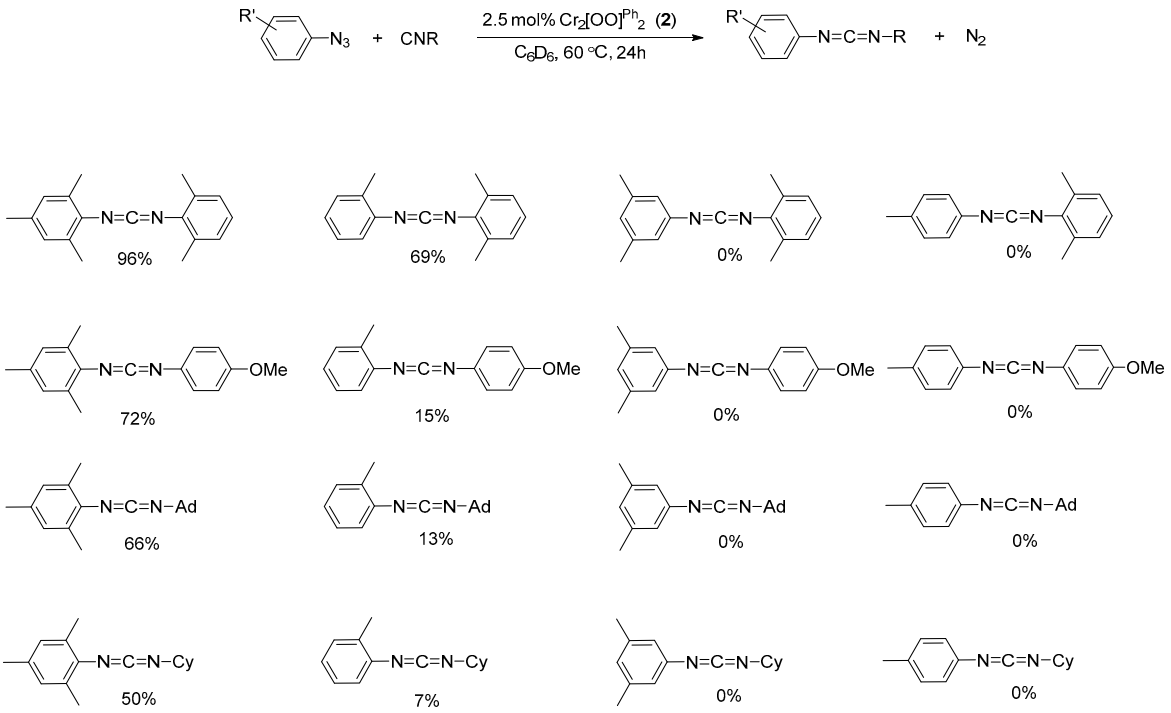

Scheme 3. Catalytic formation of carbodiimides mediated by **2**.

3. Materials and Methods

3.1. General

$CrCl_2$ and $LiN(Si(CH_3)_3)_2$ were purchased from Strem chemicals and Sigma-Aldrich, respectively, and used as received. Previously reported methods were used to synthesize $Cr(N(SiMe_3)_2)_2(THF)_2$ and the ligand precursor $H_2[OO]^{Ph}$ [35,51]. Deuterated solvents were purchased from Cambridge Isotope Laboratories and stored over 3 Å molecular sieves. Non-deuterated solvents were purchased from Sigma-Aldrich chemicals and purified using MBraun solvent purification system. Characterization of compounds was carried out using ^1H and ^{13}C NMR spectroscopy, high-resolution mass spectrometry and elemental analysis. Selected chemicals were characterized by X-ray crystallography. NMR spectra of carbodiimides and complexes were recorded using Agilent 400 MHz and Agilent DD2 600 MHz spectrometers, respectively, in C_6D_6 at room temperature at the Lumigen Instrument Center. Chemical shifts and coupling constants (J) are reported in parts per million and Hertz, respectively. Elemental analyses were carried out by Midwest Microlab LLC under air-free conditions. A Thermo Fisher Scientific LTQ Orbittrap XL mass spectrometer at the Lumigen Instrument Center was used for high resolution mass spectra. IR spectra of powdered samples were recorded on a Shimadzu IR Affinity-1 FT-IR spectrometer outfitted with a MIRacle10 attenuated total reflectance accessory with a monolithic diamond crystal stage and pressure clamp. A Shimadzu UV-1800 spectrometer was used to collect UV–Vis spectra. All air-sensitive reactions were carried out in a nitrogen-filled glovebox.

3.2. Synthesis of Cr Complexes **1**–**6** and Compound **7**

$Cr_2([OO]^{Ph})_2$ and $Cr[OO]^{Ph}(THF)_2$ (1 and 2). A solution of ligand precursor $H_2[OO]^{Ph}$ (0.034 g, 0.057 mmol) in THF (5 mL) was added to a solution of $Cr(N(SiMe_3)_2)_2(THF)_2$ (0.030 g, 0.057 mmol) in THF (5 mL). The color of the reaction changed from purple to light green over a course of 4 h. The solvent was removed under vacuum and the resulting residue recrystallized in DCM-THF mixture at −35 °C to obtain light green crystals of **2** in 79% yield (0.029 g, 0.023 mmol). Anal. Calcd for $C_{88}H_{64}Cr_2O_4$: C, 81.97, H, 5.00. Found: C, 80.82, H, 6.23. λ_{max} (ε_M (L^{-1} cm^{-1} mol^{-1})) 706 nm (28000). IR (cm^{-1}): 2947 (m), 2337 (m), 1334 (w), 1151 (w), 987 (m), 840 (m), 756 (s), 702 (s). A similar procedure was used to synthesize $Cr[OO]^{Ph}$ $(THF)_2$ (**1**) but recrystallization was done in toluene with small amount of THF. Calcd for $C_{52}H_{46}CrO_4$: C, 79.17, H, 6.13. Found C, 78.37, H, 5.39. IR (cm^{-1}) 2916 (m), 2353 (m), 1458 (m), 1365 (w), 1319 (w), 1149 (w), 1026 (m), 995 (w), 833 (m), 779 (s), 740 (m), 709 (m), 686 (m).

Synthesis of $Cr[OO]^{Ph}(N(4\text{-}CH_3C_6H_4))_2$ (3, Figure 6). A solution of 4-azidotoluene (0.020 g, 0.15 mmol) in THF was added to a 5 mL solution of $Cr_2([OO]^{Ph})_2$ (0.050 g, 0.038 mmol). Upon addition, the solution color changed from light green to brown; the release of N_2 was also observed. The reaction was stirred for 24 h. The solvent was removed under vacuum and the solid residue was recrystallized from ether-THF mixture at −35 °C to afford dark brown crystals in 69% yield (0.046 g, 0.054 mmol). ^{1}H NMR (600 MHz, C_6D_6, 298 K): δ 7.58 (d, 2H, J_{HH} = 7.6 Hz, H_a), 7.6 (d, 8H, J_{HH} = 6.1 Hz, H_f), 7.41 (s, 4H, H_e), 7.10-7.12 (m, 2H, H_b), 7.03-7.07 (m, 12H, H_g & H_h), 6.93-6.96 (m, 4H, H_c & H_d), 6.53 (d, 4H, J_{HH} = 7.6 Hz, H_j, 6.15 (d, 4H, J_{HH} = 8.2 Hz, H_i), 1.92 (s, 6H, H_k). ^{13}C NMR (150 MHz, C_6D_6, 298 K): δ 160.69, 151.19, 146.27, 142.97, 142.93, 137.30, 131.11, 130.92, 129.17, 128.22, 127.92, 127.55, 127.52, 127.37, 126.39, 125.57, 124.26, 95.51, 20.72.

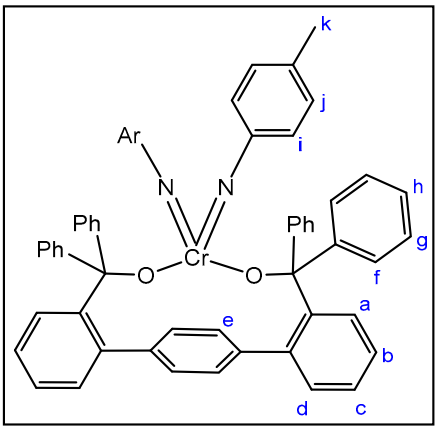

Figure 6. Assignment of ^{1}H NMR signals for **3** (see previous paragraph for details).

$Cr[OO]^{Ph}(N(4\text{-}CH_3OC_6H_4))_2$ (4, Figure 7). A solution of 4-azidoanisole (0.023 g, 0.15 mmol in THF) was added to a 5 mL THF solution of $Cr_2([OO]^{Ph})_2$ (0.050 g, 0.038 mmol). Color changed from light green to brown with release of N_2 and the reaction was stirred for 24 h. The solvent was removed under vacuum and the resulting residue was recrystallized from ether/THF mixture at −35 °C to give a brown solid, which was washed with ether to afford the product in 54% yield (0.54 g, 0.043 mmol). ^{1}H NMR (600 MHz, C_6D_6, 298 K): δ 7.57–7.61 (m, 10H, H_a and H_f), 7.44 (s, 4H, H_e), 7.10–7.12 (m, 2H, H_b), 7.02–7.08 (t, 8H, J_{HH} = 7.0 Hz, H_g), 7.01–7.03 (t, 4H, J_{HH} = 7.0 Hz, H_h), 6.97 (m, 4H, H_c and H_d), 6.31 (d, 4H, J_{HH} = 8.8 Hz, H_j), 6.27 (d, 4H, J_{HH} = 8.8 Hz, H_i), 3.07 (s, 6H, H_k). ^{13}C NMR (150 MHz, C_6D_6, 298 K): δ 158.54, 157.54, 151.30, 146.41, 143.00, 131.08, 130.95, 129.21, 127.92, 127.71, 127.54, 127.52, 127.31, 126.32, 126.13, 125.54, 112.79, 95.07, 54.91.

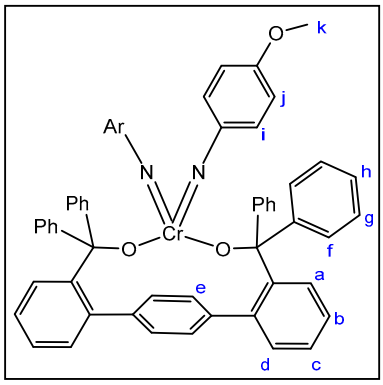

Figure 7. Assignment of ^{1}H NMR signals for **4** (see previous paragraph for details).

Cr[OO]^{Ph}(N(3,5-Me$_2$C$_6$H$_3$))$_2$ (5, Figure 8). A solution of 3,5-dimethylphenyl azide (0.022 g, 0.15 mmol) in THF) was added to THF solution (5 mL) of Cr$_2$([OO]^{Ph})$_2$ (0.050 g, 0.038 mmol). Color changed from light green to brown with release of N_2 and the reaction was stirred for 24 h. The solvent was removed under vacuum and the residue was recrystallized from ether-THF at −35 °C to form a brown solid, which was washed with ether to afford the product in 57% (0.038 g, 0.043 mmol). ^{1}H NMR (600 MHz, C_6D_6, 298 K) δ 7.57–7.61 (m, 10H, H_a and H_f), 7.42 (s, 4H, H_e), 7.09–7.11, (2H, t, J_{HH} = 6.4 Hz, H_b), 7.00–7.08 (m, 12H, H_g and H_h), 6.93 (t, 2H, J_{HH} = 7.6 Hz, H_c), 6.90 (d, 2H, J_{HH} = 8.8 Hz, H_d), 6.31 (s, 2H, H_k), 5.84 (s, 4H, H_i), 1.82 (s, 12H, H_j). ^{13}C NMR (150 MHz, C_6D_6, 298K): δ 162.5, 151.20, 146.26, 142.97, 136.83, 131.11, 130.94, 129.21, 129.14, 128.98, 128.19, 127.92, 126.96, 126.75, 126.44, 126.20, 125.55, 121.99, 95.52. 20.37.

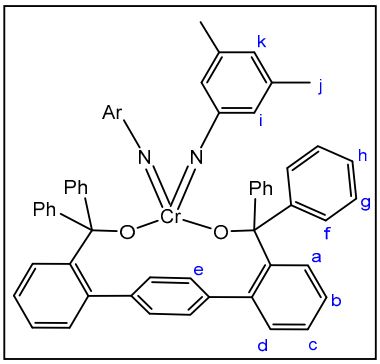

Figure 8. Assignment of ^{1}H NMR signals for **5** (see previous paragraph for details).

Cr[OO]Ph(N$_2$CPh$_2$)$_2$ (6). A (5 mL) THF solution of Cr$_2$([OO]^{Ph})$_2$ (0.030 g, 0.023 mmol) was reacted with diphenyldiazomethane (0.018 g, 0.092 mmol) for 4 h. The light green color of the complex changed immediately to purple. The solution was stirred for 6 h at RT. The solvent was removed under vacuum and the residue was recrystallized from ether-THF mixture at −35 °C. Brown color crystals were isolated in 52% yield (0.025 g, 0.024 mmol). Calcd for $C_{70}H_{52}CrN_4O_2\times C_4H_8O\times 0.5C_6H_{12}$: C, 80.60, H, 5.80. Found C, 79.52, H, 5.57.

6,6,12,12-tetraphenyl-6,12-dihydroindeno[1,2-b]fluorene (7, Figure 9). 1. Reaction of Cr$_2$-([OO]^{Ph})$_2$ with (NO)(BF$_4$): A solution of (NO)(BF$_4$) (0.010 g, 0.093 mmol) in THF (5 mL) was added to a THF solution (5 mL) of Cr$_2$([OO]^{Ph})$_2$ (0.030 g, 0.023 mmol). The green color solution became cloudy and turned yellow over the course of 6 h. The solvent was removed under vacuum and the residue recrystallized with ether-THF mixture. Colorless crystals were obtained in 92% yield (0.023 g, 0.040 mmol). 2. Reaction of H$_2$[OO]^{Ph} with (NO)(BF$_4$): A solution of (NO)(BF$_4$) (0.012 g, 0.1 mmol) in THF (5 mL) was added to a THF solution (5 mL) of H$_2$[OO]^{Ph} (0.030 g, 0.051 mmol). The colorless solution turned light brown over a period of 6 h. The solvent was removed under vacuum and the

residue recrystallized in CH_2Cl_2. Colorless crystals of **7** were obtained in 77% yield (0.021 g, 0.039 mmol). ^{1}H NMR (600 MHz, CD_2Cl_2, 298 K): δ 7.81 (s, 2H, He), 7.71 (d, J_{HH} = 7.6 Hz, 2H, H_a), 7.38 (d, 2H, J_{HH} = 7.6, H_d), 7.32 (t, 2H, J_{HH} = 7.6 Hz, H_b), 7.26 (m, 22H, H_c, H_f, H_g, H_h). Related compound (lacking the phenyl substituents) and its NMR characterization were previously reported [50]. ^{13}C NMR (125 MHz, CD_2Cl_2, 298K): δ 151.48, 151.12, 145.92, 140.21, 139.93, 128.27, 128.13, 127.58, 127.48, 126.69, 126.07, 120.16, 117.81, 65.24. HRMS (m/z): Calcd, $[C_{44}H_{30}]^+$ 558.2347, found 558.2333.

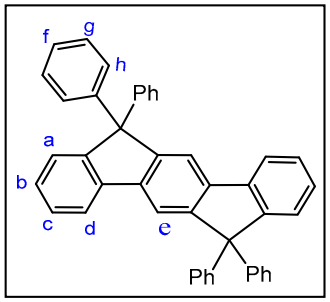

Figure 9. Assignment of ^{1}H NMR signals for **7** (see previous paragraph for details).

General Procedure for Catalytic Studies. C_6D_6 solution containing 20 equivalents of an organoazide, 24 equivalents of an isocyanide and 2 equivalents of 1,3,5-trimethoxybenzene (internal standard) was mixed with 2.5 mol% catalyst in C_6D_6. The reaction was heated at 60 °C for 24 h. The products were identified, and the yields were calculated using ^{1}H NMR spectroscopy.

3.3. X-ray Crystallographic Details

Structures of complexes **1**, **2**, **3**, and **6**, and 6,6,12,12-tetraphenyl-6,12-dihydroindeno-[1,2-b] fluorene (**7**) were confirmed by X-ray structure determination; data collection and refinement details are given in Table 1. The crystals were mounted on a Bruker APEXII/Kappa three circle goniometer platform diffractometer equipped with an APEX-2 detector. The structures of **1**, **3**, **6**, and **7** were collected using MoKα (λ = 0.71073 Å) at Wayne State University. The structure of **2** was collected using CuKα radiation (1.54178 Å) in the Center for Crystallographic Research in the Department of Chemistry, Michigan State University. The data were processed and refined using the APEX2 software. Structures were solved by direct methods in SHELXS and refined by standard difference Fourier techniques in the SHELXTL program suite (6.10 v., Sheldrick G. M., and Siemens Industrial Automation, 2000). Hydrogen atoms were placed in calculated positions using the standard riding model and refined isotropically; all other atoms were refined anisotropically. The structure of **6** contained half a molecule of cyclohexane and a molecule of THF in the asymmetric unit. The structure of **7** co-crystallized with CH_2Cl_2 which was fully refined. The structure of **3** contained multiple severely disordered THF solvent molecules in the asymmetric unit, leading to the overall poor quality of the diffraction data. We had only limited success in modelling the disorder in THF solvent, thus, SQUEEZE program was applied to remove the disordered solvent. One of the *para*-tolyl groups in the structure of **3** was found to be disordered; the disorder was successfully modeled by finding two alternative conformations. The structure of **1** was also of relatively poor quality, due to the very small size of the crystals. Despite data collection at 60 s per frame, little diffraction was observed beyond ~1 Å. The structure of **1** contained several toluene molecules per asymmetric unit, one of which was found to be disordered over two conformations. The structure of **2** contained significant amount of highly disordered THF solvent, which was removed using SQUEEZE.

Table 1. X-ray crystallographic details for complexes **1**–**3**, **6**, and compound **7**.

Complex	1	2	3	6	7
formula	$C_{52}H_{46}CrO_4 \times 2.5C_7H_8$	$2C_{88}H_{64}Cr_2O_4$	$C_{58}H_{46}CrN_2O_2$	$C_{70}H_{52}CrN_4O_2 \times 0.5C_6H_{12} \times C_4H_8O$	$C_{22}H_{15} \times CH_2Cl_2$
fw, g/mol	1020.25	2578.80	854.97	1147.34	364.27
crystal system	Triclinic	Triclinic	Monoclinic	Triclinic	Triclinic
space group	*P*-1	*P*-1	*P*21/c	*P*-1	*P*-1
a (Å)	9.946 (11)	13.9851 (4)	17.38 (15)	10.1831 (6)	8.7464 (5)
b (Å)	14.298 (16))	19.4602 (6)	13.03 (11)	13.0107 (7)	8.7610 (5)
c (Å)	19.19 (2)	30.4287 (10)	28.58 (19)	23.0961 (13)	12.4072 (7)
α (deg)	83.38 (3)	81.683 (2)	90.00	100.964 (3)	76.995 (2)
β (deg)	82.55 (2)	77.609 (2)	127.4 (4)	101.580 (3)	78.928 (2)
γ (deg)	82.44 (2)	74.125 (2)	90.00	99.999 (3)	70.505 (2)
V (Å^3)	2668 (5)	7747.2 (4)	5142 (71)	2870.7 (3)	866.13 (9)
Z	2	4	4	2	2
d_{calcd}, g/cm^3	1.270	1.1055	1.104	1.327	1.397
μ, mm^{-1}	0.266	2.673	0.263	0.257	0.377
T (K)	100(2)	172.99	100 (2)	100 (2)	100 (2)
2θ, deg	49.00	128.14	47.44	52.96	55.02
R_1[a] [(I > 2σ)]	0.0981	0.0827	0.0727	0.0730	0.0388
wR_2[b] [(I > 2σ)]	0.2070	0.1875	0.1512	0.1710	0.0803
GOF[c] (F^2)	0.973	0.7573	0.881	1.037	1.041

[a] $R_1 = \sum||F_o| - |F_c||/\sum|F_o|$. [b] $wR_2 = (\sum (w(F_o^2 - F_c^2)^2)/\sum(w(F_o^2)^2))^{1/2}$. [c] GOF = $(\sum w(F_o^2 - F_c^2)^2/(n-p))^{1/2}$, where *n* is the number of data and *P* is the number of parameters refined.

3.4. Computational Details

DFT calculations were performed using Gaussian 09 [52]. All calculations were performed at the BP86-D3/def2-SVP level of theory [53–57], employing density fitting, ultrafine grids [58], and Becke–Johnson damping for the dispersion corrections. Optimized structures were confirmed to be minima by ensuring all harmonic frequencies were real. All wavefunctions were verified to be stable. Orbital analyses were performed in GaussView 6.0.16 [59], and Mayer bond orders were calculated using Multiwfn 3.5 [60].

4. Conclusions

We have demonstrated that chelating bis(alkoxide) ligand $[OO]^{Ph}$, featuring a terphenyl spacer between the alkoxide donors, forms mononuclear ($Cr[OO]^{Ph}(THF)_2$) or dinuclear ($Cr_2[OO]^{Ph}{}_2$) Cr(II) complexes, depending on the crystallization conditions. These results suggest that $[OO]^{Ph}$ exhibits a larger steric profile compared with two monodentate alkoxides [OC^tBu_2Ph] that formed a $Cr_2(OC^tBu_2Ph)_4$ dimer invariably. Reactions of this complex with organoazides form diamagnetic Cr(VI) bis(imido) complexes or paramagnetic Cr(IV) mono(imido) complexes. The outcome of the reaction depends on the sterics of the organoazide: mesityl azide formed Cr(IV) mono(imido) but 3,5-dimethylphenyl/4-methylphenyl azides formed Cr(VI) bis(imido) complexes. With diphenyldiazomethane, a chromium bis(diphenylmethylenehydrazido) product forms. Treatment of the Cr(II) precursor with isocyanide likely forms a Cr(II) isocyanide adduct, whereas no reaction is observed with CO. Isoelectronic nitrosonium abstracts hydroxyl to induce cyclization, producing 6,6,12,12-tetraphenyl-6,12-dihydroindeno[1,2-b]fluorene. Catalytic studies combining mixtures of isocyanides with organozides enable carbodiimide formation only for bulkier (mono- or di-orthosubstituted) aryl azides. This finding is consistent with our previous report, which demonstrated that the C–N bond formation in carbodiimide is preceded by isocyanide coordination to the metal and thus occurs at the Cr(IV) mono(imido) intermediate only. Our future studies will focus on the development of new chelating bis(alkoxide) ligands, which could enable catalytic reactivity for a wider range of substrates.

Supplementary Materials: The following are available online: NMR, MS, UV–Vis and IR spectra, cif files, and computational details. Cif files of the structures of **1–3**, **6**, and **7** were deposited at CCDC under the following numbers: 1970958–1970962.

Author Contributions: Conceptualization: S.S.K., R.L.L., and S.G.; methodology: S.S.K., R.J.S., R.L.L., and S.G.; writing—original draft preparation, S.S.K., R.L.L., and S.G.; writing—review and editing, S.S.K. and R.L.L.; supervision: R.L.L. and S.G.; funding acquisition: R.L.L., S.G., and R.J.S. All authors have read and agreed to the published version of the manuscript.

Funding: This research was funded by National Science Foundation, Division of Chemistry, grant number CHE 1855681. Grand Valley State University Libraries are acknowledged for their financial support of this open access publication.

Acknowledgments: Compounds characterization was carried out at Lumigen Instrument Center, Wayne State University. The CCD based X-ray diffractometer at Michigan State University were upgraded and/or replaced by departmental funds. We thank Amanda Grass and Duleeka Wannipurage for technical assistance.

Conflicts of Interest: The authors declare no conflict of interest.

References

1. Jenkins, D.M. Atom-Economical C_2 + N_1 aziridination: Progress towards catalytic intermolecular reactions using alkenes and aryl azides. *Synlett* **2012**, *23*, 1267–1270. [CrossRef]
2. Driver, T.G. Recent advances in transition metal-catalyzed N-Atom transfer reactions of azides. *Org. Biomol. Chem.* **2010**, *8*, 3831–3846. [CrossRef]
3. Shin, K.; Kim, H.; Chang, S. Transition-Metal-Catalyzed C-N Bond forming reactions using organic azides as the nitrogen source: A journey for the mild and versatile C-H Amination. *Acc. Chem. Res.* **2015**, *48*, 1040–1052. [CrossRef]
4. Wang, P.; Deng, L. Recent advances in iron-catalyzed C-H bond amination via iron imido intermediate. *Chin. J. Chem.* **2018**, *36*, 1222–1240. [CrossRef]
5. Lu, H.; Zhang, X.P. Catalytic C–H functionalization by metalloporphyrins: Recent developments and future directions. *Chem. Soc. Rev.* **2011**, *40*, 1899–1909. [CrossRef] [PubMed]
6. Uchida, T.; Katsuki, T. Asymmetric nitrene transfer reactions: Sulfimidation, aziridination and C–H amination using azide compounds as nitrene precursors. *Chem. Rec.* **2014**, *14*, 117–129. [CrossRef] [PubMed]
7. Kuijpers, P.F.; van der Vlugt, J.I.; Schneider, S.; de Bruin, B. Nitrene radical intermediates in catalytic synthesis. *Chem. Eur. J.* **2017**, *23*, 13819–13829. [CrossRef]
8. Baek, Y.; Hennessy, E.T.; Betley, T.A. Direct manipulation of metal imido geometry: Key principles to enhance C–H amination efficacy. *J. Am. Chem. Soc.* **2019**, *141*, 16944–16953. [CrossRef]
9. Wilding, M.J.T.; Iovan, D.A.; Betley, T.A. High-Spin iron imido complexes competent for C–H bond amination. *J. Am. Chem. Soc.* **2017**, *139*, 12043–12049. [CrossRef]
10. Cheng, J.; Liu, J.; Leng, X.; Lohmiller, T.; Schnegg, A.; Bill, E.; Ye, S.; Deng, L. A Two-Coordinate iron(II) imido complex with NHC ligation: Synthesis, characterization, and its diversified reactivity of nitrene transfer and C–H bond activation. *Inorg. Chem.* **2019**, *58*, 7634–7644. [CrossRef]
11. Du, J.; Wang, L.; Xie, M.; Deng, L. A Two-Coordinate cobalt(II) imido complex with NHC ligation: Synthesis, structure, and reactivity. *Angew. Chem. Int. Ed.* **2015**, *54*, 12640–12644. [CrossRef] [PubMed]
12. Cowley, R.E.; Golder, M.R.; Eckert, N.A.; Al-Afyouni, M.H.; Holland, P.L. Mechanism of catalytic nitrene transfer using iron(I)-isocyanide complexes. *Organometallics* **2013**, *32*, 5289–5298. [CrossRef]
13. Bagh, B.; Broere, D.L.J.; Sinha, V.; Kuijpers, P.F.; van Leest, N.P.; de Bruin, B.; Demeshko, S.; Siegler, M.A.; van der Vlugt, J.I. Catalytic synthesis of N-heterocycles via direct C(sp3)–H amination using an air-stable iron(III) species with a redox-active ligand. *J. Am. Chem. Soc.* **2017**, *139*, 5117–5124. [CrossRef] [PubMed]
14. Vreeken, V.; Baij, L.; de Bruin, B.; Siegler, M.A.; van der Vlugt, J.I. N-Atom transfer via thermal or photolytic activation of a Co-azido complex with a PNP pincer ligand. *Dalton Trans.* **2017**, *46*, 7145–7149. [CrossRef] [PubMed]
15. Hakey, B.M.; Darmon, J.M.; Akhmedov, N.G.; Petersen, J.L.; Milsmann, C. Reactivity of pyridine dipyrrolide iron(II) complexes with organic azides: C–H amination and iron tetrazene formation. *Inorg. Chem.* **2019**, *58*, 11028–11042. [CrossRef]
16. Goswami, M.; de Bruin, B. Porphyrin Co(III)-nitrene radical mediated pathway for synthesis of o-aminoazobenzenes. *Molecules* **2018**, *23*, 1052. [CrossRef]

17. Mankad, N.P.; Müller, P.; Peters, J.C. Catalytic N−N coupling of aryl azides to yield azoarenes via trigonal bipyramid iron−nitrene intermediates. *J. Am. Chem. Soc.* **2010**, *132*, 4083–4085. [CrossRef]
18. Lang, K.; Torker, S.; Wojtas, L.; Zhang, X.P. Asymmetric induction and enantiodivergence in catalytic radical C–H Amination via enantiodifferentiative H-Atom abstraction and stereoretentive radical substitution. *J. Am. Chem. Soc.* **2019**, *141*, 12388–12396. [CrossRef]
19. Jacobs, B.P.; Wolczanski, P.T.; Jiang, Q.; Cundari, T.R.; MacMillan, S.N. Rare examples of Fe(IV) alkyl-imide migratory insertions: Impact of Fe-C covalency in $(Me_2IPr)Fe(=NAd)R_2$ (R = neoPe, 1-nor). *J. Am. Chem. Soc.* **2017**, *139*, 12145–12148. [CrossRef]
20. Powers, I.G.; Andjaba, J.M.; Luo, X.; Mei, J.; Uyeda, C. catalytic azoarene synthesis from aryl azides enabled by a dinuclear Ni complex. *J. Am. Chem. Soc.* **2018**, *140*, 4110–4118. [CrossRef]
21. Spasyuk, D.M.; Carpenter, S.H.; Kefalidis, C.E.; Piers, W.E.; Neidig, M.L.; Maron, L. Facile hydrogen atom transfer to Iron(III) imido radical complexes supported by a dianionic pentadentate ligand. *Chem. Sci.* **2016**, *7*, 5939–5944. [CrossRef] [PubMed]
22. Nugent, W.A.; Mayer, J.M. *Metal-Ligand Multiple Bonds: The Chemistry of Transition Metal Complexes Containing Oxo, Nitrido, Imido, Alkylidene, or Alkylidyne Ligands*, 1st ed.; Wiley-Interscience: New York, NY, USA, 1988.
23. Danopoulos, A.A.; Hussain-Bates, B.; Hursthouse, M.B.; Leung, W.H.; Wilkinson, G. t-Butylimido complexes of chromium(V). X-ray crystal structure of t-butylimidotrichlorobis(ethyldiphenylphosphine)chromium(V). *J. Chem. Soc. Chem. Commun.* **1990**, *23*, 1678–1679. [CrossRef]
24. Danopoulos, A.A.; Hankin, D.M.; Wilkinson, G.; Cafferkey, S.M.; Sweet, T.K.N.; Hursthouse, M.B. Amido, imido and carbene complexes of chromium. *Polyhedron* **1997**, *16*, 3879–3892. [CrossRef]
25. Edwards, N.Y.; Eikey, R.A.; Loring, M.I.; Abu-Omar, M.M. High-Valent imido complexes of manganese and chromium corroles. *Inorg. Chem.* **2005**, *44*, 3700–3708. [CrossRef] [PubMed]
26. Wu, P.; Yap, G.P.A.; Theopold, K.H. Structure and reactivity of chromium(VI) alkylidenes. *J. Am. Chem. Soc.* **2018**, *140*, 7088–7091. [CrossRef] [PubMed]
27. Leung, W.-H. Synthesis and reactivity of organoimido complexes of chromium. *Eur. J. Inorg. Chem.* **2003**, 583–593. [CrossRef]
28. Beaumier, E.P.; Billow, B.S.; Singh, A.K.; Biros, S.M.; Odom, A.L. A complex with nitrogen single, double, and triple bonds to the same chromium atom: Synthesis, structure, and reactivity. *Chem. Sci.* **2016**, *7*, 2532–2539. [CrossRef]
29. Keller, C.L.; Kern, J.L.; Terry, B.D.; Roy, S.; Jenkins, D.M. Catalytic aziridination with alcoholic substrates via a chromium tetracarbene catalyst. *Chem. Commun.* **2018**, *54*, 1429–1432. [CrossRef]
30. Elpitiya, G.R.; Malbrecht, B.J.; Jenkins, D.M. A Chromium(II) tetracarbene complex allows unprecedented oxidative group transfer. *Inorg. Chem.* **2017**, *56*, 14101–14110. [CrossRef]
31. Yousif, M.; Tjapkes, D.J.; Lord, R.L.; Groysman, S. Catalytic formation of asymmetric carbodiimides at mononuclear Chromium (II/IV) bis(alkoxide) complexes. *Organometallics* **2015**, *34*, 5119–5128. [CrossRef]
32. Heins, S.P.; Morris, W.D.; Wolczanski, P.T.; Lobkovsky, E.B.; Cundari, T.R. Nitrene insertion into C-C and C-H bonds of diamide diimine ligands ligated to chromium and iron. *Angew. Chem. Int. Ed.* **2015**, *54*, 14407–14411. [CrossRef] [PubMed]
33. Bellow, J.A.; Yousif, M.; Groysman, S. Discrete complexes of 3d metals with monodentate bulky alkoxide ligands and their reactivity in bond activation and bond formation reactions. *Comments Inorg. Chem.* **2015**, *36*, 92–122. [CrossRef]
34. Grass, A.; Wannipurage, D.; Lord, R.L.; Groysman, S. Group-transfer chemistry at transition metal centers in bulky alkoxide ligand environments. *Coord. Chem. Rev.* **2019**, *400*, 1–16. [CrossRef]
35. Kurup, S.S.; Wannipurage, D.; Lord, R.L.; Groysman, S. An iron complex with a new chelating bis(alkoxide) ligand leads to an active nitrene dimerization catalyst for a variety of para- and meta-substituted azide precursors. *Chem. Commun.* **2019**, *55*, 10780–10783. [CrossRef] [PubMed]
36. Yousif, M.; Wannipurage, D.; Huizenga, C.D.; Washnock-Schmid, E.; Peraino, N.J.; Ozarowski, A.; Stoian, S.A.; Lord, R.L.; Groysman, S. Catalytic nitrene homocoupling by an iron(II) bis(alkoxide) complex: Bulking up the alkoxide enables a wider range of substrates and provides insight into the reaction mechanism. *Inorg. Chem.* **2018**, *57*, 9425–9438. [CrossRef] [PubMed]
37. Bellow, J.A.; Yousif, M.; Cabelof, A.C.; Lord, R.L.; Groysman, S. Reactivity modes of an iron bis(alkoxide) complex with aryl azides: Catalytic nitrene coupling vs formation of iron(III) imido dimers. *Organometallics* **2015**, *34*, 2917–2923. [CrossRef]

38. Yousif, M.; Cabelof, A.C.; Martin, P.D.; Lord, R.L.; Groysman, S. Synthesis of a mononuclear, non-square-planar chromium(ii) bis(alkoxide) complex and its reactivity toward organic carbonyls and CO_2. *Dalton Trans.* **2016**, *45*, 9794–9804. [CrossRef]
39. Murray, B.D.; Hope, H.; Power, P.P. An Unusual C-C Bond cleavage in a bulky metal alkoxide: Syntheses and X-ray crystal structures of three-coordinate Mn(II) and Cr(II) complexes containing the di-tert-butylmethoxide ligand. *J. Am. Chem. Soc.* **1985**, *107*, 169–173. [CrossRef]
40. Sydora, O.L.; Kuiper, D.S.; Wolczanski, P.T.; Lobkovsky, E.B.; Dinescu, A.; Cundari, T.R. The butterfly dimer [(tBu3SiO)Cr]2(μ-OSitBu3)2 and its oxidative cleavage to (tBu3SiO)2Cr(N−NCPh2)2 and (tBu3SiO)2CrN(2,6-Ph2-C6H3). *Inorg. Chem.* **2006**, *45*, 2008–2021. [CrossRef]
41. Ohki, Y.; Takikawa, Y.; Hatanaka, T.; Tatsumi, K. Reductive N−N Bond cleavage of diphenylhydrazine and azobenzene induced by coordinatively unsaturated Cp*Fe{$N(SiMe_3)_2$}. *Organometallics* **2006**, *25*, 3111–3113. [CrossRef]
42. Bellows, S.M.; Arnet, N.A.; Gurubasavaraj, P.M.; Brennessel, W.W.; Bill, E.; Cundari, T.R.; Holland, P.L. The Mechanism of N-N double bond cleavage by an Iron(II)-hydride complex. *J. Am. Chem. Soc.* **2016**, *138*, 12112–12123. [CrossRef] [PubMed]
43. Davis-Gilbert, Z.W.; Wen, X.; Goodpaster, J.D.; Tonks, I.A. Mechanism of Ti-catalyzed oxidative nitrene transfer in [2 + 2 + 1] pyrrole synthesis from alkynes and azobenzene. *J. Am. Chem. Soc.* **2018**, *140*, 7267–7281. [CrossRef]
44. Kawakita, K.; Beaumier, E.P.; Kakiuchi, Y.; Tsurugi, H.; Tonks, I.A.; Mashima, K. Bis(imido)vanadium(V)-catalyzed [2 + 2 + 1] coupling of alkynes and azobenzenes giving multisubstituted pyrroles. *J. Am. Chem. Soc.* **2019**, *141*, 4194–4198. [CrossRef] [PubMed]
45. Copéret, C.; Comas-Vives, A.; Conley, M.P.; Estes, D.P.; Fedorov, A.; Mougel, V.; Nagae, H.; Núñez-Zarur, F.; Zhizhko, P.A. surface organometallic and coordination chemistry toward single-site heterogeneous catalysts: Strategies, methods, structures, and activities. *Chem. Rev.* **2016**, *116*, 323–421. [CrossRef] [PubMed]
46. Wu, P.; Yap, G.P.A.; Theopold, K.H. Synthesis, characterization, and reactivity of chromium(VI) alkylidenes. *Organometallics* **2019**, *38*, 4593–4600. [CrossRef]
47. Grass, A.; Dewey, N.S.; Lord, R.L.; Groysman, S. Ketenimine formation catalyzed by a high valent cobalt carbene in bulky alkoxide ligand environment. *Organometallics* **2019**, *38*, 962–972. [CrossRef]
48. Grass, A.; Stoian, S.A.; Lord, R.L.; Groysman, S. Transition metal-mediated reductive coupling of diazoesters. *Chem. Commun.* **2019**, *55*, 8458–8461. [CrossRef]
49. Hempe, M.; Reggelin, M. Molecular Packing and Morphological Stability of Dihydro-indeno[1,2-b]fluorenes in the Context of Their substitution Pattern. *RSC Adv.* **2017**, *7*, 47183–47189. [CrossRef]
50. Poriel, C.; Liang, J.-J.; Rault-Berthelot, J.; Barrière, F.; Cocherel, N.; Slawin, A.M.Z.; Horhant, D.; Virboul, M.; Alcaraz, G.; Audebrand, N.; et al. Dispirofluorene–Indenofluorene derivatives as new building blocks for blue organic electroluminescent devices and electroactive polymers. *Chem. Eur. J.* **2007**, *13*, 10055–10069. [CrossRef]
51. Bradley, D.C.; Hursthouse, M.B.; Newing, C.W.; Welch, A. Square planar and tetrahedral chromium(II) complexes; crystal structure determinations. *J. Chem. Soc. Chem. Commun.* **1972**, 567–568. [CrossRef]
52. Frisch, M.J.; Trucks, G.W.; Schlegel, H.B.; Scuseria, G.E.; Robb, M.A.; Cheeseman, J.R.; Scalmani, G.; Barone, V.; Mennucci, B.; Petersson, G.A.; et al. *Gaussian 09*; revision D.01; Gaussian, Inc.: Wallingford, CT, USA, 2009.
53. Becke, A.D. Density-functional exchange-energy approximation with correct asymptotic behavior. *Phys. Rev. A* **1988**, *38*, 3098–3100. [CrossRef] [PubMed]
54. Perdew, J.P. Density-functional approximation for the correlation energy of the inhomogeneous electron gas. *Phys. Rev. B* **1986**, *33*, 8822–8824. [CrossRef] [PubMed]
55. Grimme, S.; Antony, J.; Ehrlich, S.; Krieg, H. A consistent and accurate ab initio parameterization of density functional dispersion correction (DFT-D) for the 94 elements H–Pu. *J. Chem. Phys.* **2010**, *132*, 154104. [CrossRef] [PubMed]
56. Grimme, S.; Ehrlich, S.; Goerigk, L. Effect of the damping function in dispersion corrected density functional theory. *J. Comput. Chem.* **2011**, *32*, 1456–1465. [CrossRef] [PubMed]
57. Weigend, F.; Ahlrichs, R. Balanced basis sets of split valence, triple zeta valence, and quadruple zeta valence quality for H to Rn: Design and assessment of accuracy. *Phys. Chem. Chem. Phys.* **2005**, *7*, 3297–3305. [CrossRef]

58. Bootsma, A.N.; Wheeler, S. Popular integration grids can result in large errors in dft-computed free energies. *ChemRxiv Preprint* **2019**. [CrossRef]
59. Dennington, R.; Keith, T.A.; Millam, J.M. *GaussView*, version 6; Semichem Inc.: Shawnee Mission, KS, USA, 2016.
60. Lu, T.; Chen, F. Multiwfn: A multifunctional wavefunction analyzer. *J. Comput. Chem.* **2012**, *33*, 580–592. [CrossRef]